Research Article | Vol. 27, No. 5 | 4 Mar 2019 | OPTICS EXPRESS 7365
Optics EXPRESS

Ultra-sharp asymmetric Fano-like resonance spectrum on Si photonic platform

H. Du,[1,*] W. Zhang,[1] C. G. Littlejohns,[1,2] S. Stankovic,[1] X. Yan,[1] D. T. Tran, [1] G. J. Sharp, [3] F. Y. Gardes,[1] D. J. Thomson,[1] M. Sorel,[3] G. Z. Mashanovich,[1] and G. T. Reed[1]

[1]*Optoelectronics Research Centre, University of Southampton, Southampton SO17 1BJ, UK*
[2]*Silicon Technologies Centre of Excellence, Nanyang Technological University, 639798, Singapore*
[3]*University of Glasgow, Glasgow, G12 8LP, UK*
[*]*H.Du@soton.ac.uk*

Abstract: In this paper, we report the generation of an ultra-sharp asymmetric resonance spectrum through Fano-like interference. This generation is accomplished by weakly coupling a high-quality factor (*Q* factor) Fabry–Pérot (FP) cavity and a low-*Q* factor FP cavity through evanescent waves. The high-*Q* FP cavity is formed by Sagnac loop mirrors, whilst the low-*Q* one is built by partially transmitting Sagnac loop reflectors. The working principle has been analytically established and numerically modelled by using temporal coupled-mode-theory (CMT), and verified using a prototype device fabricated on the 340 nm silicon-on-insulator (SOI) platform, patterned by deep ultraviolet (DUV) lithography. Pronounced asymmetric resonances with slopes up to 0.77 dB/pm have been successfully measured, which, to the best of our knowledge, is higher than the results reported in state-of-the-art devices in on-chip integrated Si photonic studies. The established theoretical analysis method can provide excellent design guidelines for devices with Fano-like resonances. The design principle can be applied to ultra-sensitive sensing, ultra-high extinction ratio switching, and more applications.

1. Introduction

Fano resonance is a phenomenon describing resonant scattering, involving interference between a discrete quantum state and a continuum state [1,2], which results in asymmetric resonances. In photonics, an optical resonance with a complex eigenfrequency can be considered as a quasi-discrete state. In recent years, Fano-like resonances in Si photonic devices are widely studied [3–5] mainly due to their desirable feature of sharp resonance spectrum, which can enhance optical transduction, switching, modulation, signal processing, optical nonreciprocity, etc [6–10]. There have been many studies of Fano-like resonance in Si photonics using configurations including a cavity and a partially-transmitting-element (PTE) coupled systems [8–12], ring and Mach–Zehnder interferometer (MZI) coupled systems [13,14], 2D photonic crystal cavities or coupled 2D photonic crystal cavities [6,15], etc. Many of these studies require high resolution patterning techniques, for example, electron-beam lithography to pattern photonic crystals, which inhibits the commercialisation of these devices. The feasibility of CMOS fabrication tools, especially DUV lithography, for fabricating photonic integrated circuits has already been proved [16–18]. Thus, it is highly desirable to demonstrate the fabrication of devices with Fano-like resonances using CMOS compatible processes, namely DUV lithography, to enable these devices to be fabricated in silicon photonics foundries. In addition, although the guidelines to design devices with Fano-like resonances are highly desirable, they are not sufficient in the published studies.

In this paper, we investigate a Fano-like resonance generation mechanism with ultra-sharp resonance line shape based on on-chip integrated silicon photonic devices, in which a high-*Q* cavity and a low-*Q* cavity are weakly coupled together through evanescent waves. The high-*Q* cavity here serves as a discrete-like state, whilst the low-*Q* cavity serves as a continuum-like

#353020 https://doi.org/10.1364/OE.27.007365
Journal © 2019 Received 29 Nov 2018; revised 19 Jan 2019; accepted 9 Feb 2019; published 27 Feb 2019

Optics EXPRESS

level. Similar mechanisms can be used to design devices with electromagnetic-induced-transparency-like (EIT-like) characteristic [19]. The two cavities are designed to be weakly coupled to introduce Fano-like interference, instead of mode splitting if they are strongly coupled. The authors utilize temporal CMT to guide the device design and discuss the weak coupling effect on the Fano-like phenomenon, which is scarcely discussed in the literature. The experimental results also successfully verify the theories; a slope of 0.77 dB/pm is realized, and the sharp slope covers a range of 23 pm with an extinction ratio of 16.45 dB. In addition, a maximum transmission change of 22.3 dB over 54 pm wavelength detuning is obtained. To the best knowledge of the authors, this paper reports a higher slope of a Fano-like resonance line shape based on integrated Si photonic devices than results from other studies, for example, a transmission variation of 17 dB over 56 pm wavelength detuning in [11] or a transmission variation of 8.5 dB over 22 pm wavelength shift in [7]. Additionally, the prototype device is patterned by DUV lithography only using a 248 nm Nikon S240 Scanner with a resolution of approximately 200 nm. For the context of the paper, theoretical analysis, numerical modeling and experimental results will be presented subsequently.

2. Theoretical analysis, numerical modeling, and device design

Figure 1 shows the schematic of the prototype device studied in this paper. A high-Q cavity and a low-Q cavity are coupled together with a coupling coefficient of μ. The low-Q cavity is connected with input and output feeding waveguides, and $1/\tau_c$ denotes the decay rate of the low-Q cavity due to waveguide coupling. a_1 and a_2 denote mode amplitude of the low-Q and high-Q cavities, with a natural resonant frequency of ω_1 and ω_2, and total loss of $1/\tau_{t1}$ and $1/\tau_{t2}$, respectively. Thus $a_i = A_i \cdot \exp[(i \cdot \omega_i - 1/\tau_{ti}) \cdot t]$, $i = 1, 2$.

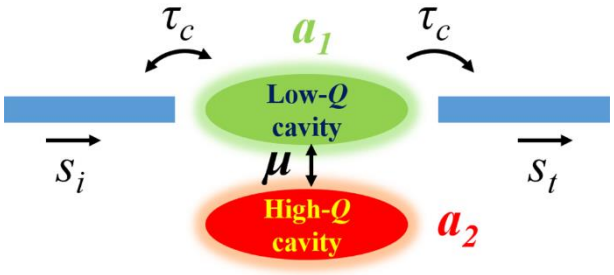

Fig. 1. Schematic of the low-Q cavity and high-Q cavity coupled configuration.

Then, the coupled-mode equations describing the coupled cavities can be written as [20,21]:

$$\frac{d}{dt}a_1 = (i \cdot \omega_1 - \frac{1}{\tau_{t1}})a_1 + \mu a_2, \tag{1}$$

$$\frac{d}{dt}a_2 = (i \cdot \omega_2 - \frac{1}{\tau_{t2}})a_2 + \mu a_1. \tag{2}$$

The eigenvalue can be solved as

$$\chi = \frac{\omega_1 + \omega_2}{2} + i \cdot \frac{1}{2}(\frac{1}{\tau_{t1}} + \frac{1}{\tau_{t2}}) \pm \sqrt{\frac{1}{4}(\Delta\omega + i \cdot \Delta\frac{1}{\tau_t})^2 + \mu^2}, \tag{3}$$

where $\Delta\omega = |\omega_1 - \omega_2|$ and $\Delta\frac{1}{\tau_t} = \left|\frac{1}{\tau_{t1}} - \frac{1}{\tau_{t2}}\right|$ and

Optics EXPRESS

$$\chi \approx \frac{\omega_1+\omega_2}{2}+i\cdot\frac{1}{2}(\frac{1}{\tau_{t1}}+\frac{1}{\tau_{t2}})\pm\sqrt{\frac{1}{4}(\Delta\omega)^2+\mu^2-\frac{1}{4}(\Delta\frac{1}{\tau_t})^2}. \quad (4)$$

When $\mu^2 > \frac{1}{4}(\Delta\frac{1}{\tau_t})^2-\frac{1}{4}(\Delta\omega)^2$, the two cavities are strongly coupled, which can cause mode splitting, whilst when $\mu^2 \le \frac{1}{4}(\Delta\frac{1}{\tau_t})^2-\frac{1}{4}(\Delta\omega)^2$, the two cavities are weakly coupled, which may introduce Fano-like interference [20–23]. However, near the transition point (, when $\mu^2 \approx \frac{1}{4}(\Delta\frac{1}{\tau_t})^2-\frac{1}{4}(\Delta\omega)^2$) the resonance line shape is also asymmetric even if it is at the strong coupling situation as defined above. Thus, fairly speaking, typical mode splitting phenomena usually happen when the cavities are ultra-strongly coupled ($\mu^2 >> \frac{1}{4}(\Delta\frac{1}{\tau_t})^2-\frac{1}{4}(\Delta\omega)^2$). The scattering matrix method is mostly used in related studies, but it is not suitable to intuitively explicate the coupling effect on the formation of Fano-like resonance. The authors believe that temporal CMT is a better method to assist device design to have Fano-like resonance. The discussion about the effect of coupling type (strong or weak coupling) on the generation of Fano-like resonance using temporal CMT in this paper fills the gap in the lack of such details among other literature.

Now we further consider the input and output of the system. s_i and s_t denote incident and transmitted waveguide mode amplitude and $s_i = S_i e^{i\omega t}$. The coupled mode equations can be written as [20]

$$\frac{d}{dt}a_1 = (i\cdot\omega_1-\frac{1}{\tau_{i1}}-\frac{1}{\tau_c})a_1+\mu a_2+\sqrt{\frac{1}{\tau_c}}s_i, \quad (5)$$

$$\frac{d}{dt}a_2 = (i\cdot\omega_2-\frac{1}{\tau_{i2}})a_2+\mu a_1, \quad (6)$$

where $1/\tau_{i1}$ and $1/\tau_{i2}$ denote the intrinsic loss of the two cavities.

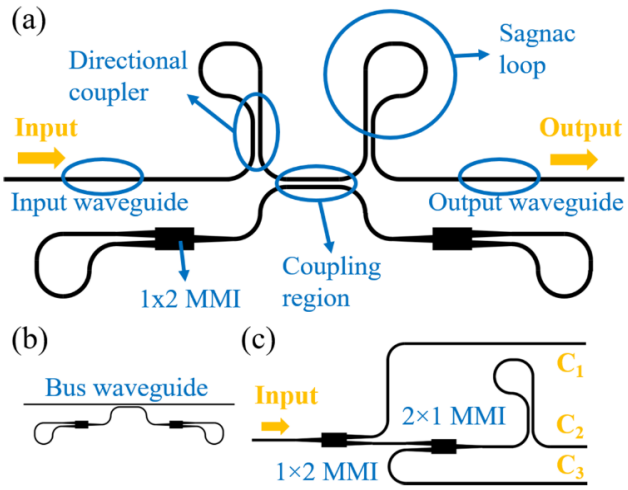

Fig. 2. (a) Schematic of the prototype device. (b) Schematic of the high-*Q* cavity device to be integrated in the prototype device. (c) Schematic of the device used to measure the reflection ratio of the PTE, which is used to form the low-*Q* cavity.

Optics EXPRESS

Figure 2(a) illustrates the prototype device configuration. The lower cavity is designed to be a high-*Q* FP cavity formed by two mirrors, each of which consists of a 1 × 2 multimode interferometer (MMI) and a Sagnac loop [24]. The MMI has an even power splitting ratio. The upper cavity is designed to be a low-*Q* FP cavity formed by two PTEs, each of which consists of a directional coupler and a Sagnac loop.

By manipulating the coupling strength of the directional coupler, the power splitting ratio can be controlled and thus the reflection and transmission coefficient of the PTE can be controlled. To be specific, assuming that the transmission and coupling coefficient of the directional coupler is t and k ($t^2 + k^2 = 1$), the amplitude transmission coefficient and reflection coefficient of the PTE can be solved as $t^2 - k^2$ and $-2itk$ respectively using scattering matrix method [24,25]. Note that when $t^2 = k^2 = 0.5$, the PTE becomes a mirror. Also note that the *Q* factor of a FP cavity is proportional to sqrt(r)/(1-r), where r is the reflection coefficient of its constituent reflectors. Consequently, by designing the coupling coefficient of the directional coupler, the *Q* factor of the low-*Q* cavity can be controlled. Figure 2(b) shows the schematic of the bare high-*Q* cavity, whilst Fig. 2(c) describes a device configuration to measure the reflection ratio of the PTE. These two devices schematised in Figs. 2(b) and 2(c) are also fabricated and measured in experiments to characterize the performance of the high-*Q* cavity and the PTE to be integrated in the proposed device with Fano-like resonances.

In the prototype device, the low-*Q* factor cavity has PTEs with low reflection coefficient. Thus, the loss due to waveguide coupling of the low-*Q* cavity dominates its total loss ($1/\tau_c \gg 1/\tau_{i1}$ and thus $1/\tau_c + 1/\tau_{i1} \approx 1/\tau_c$). The normalized amplitude transmission ($t = s_t/s_i$) of the device can be solved from Eqs. (5) and (6) as

$$t = \frac{\omega}{2Q_c} \cdot \frac{i\cdot\omega - (i\cdot\omega_2 - \frac{\omega_2}{2Q_2})}{\left[i\cdot\omega - (i\cdot\omega_1 - \frac{\omega}{2Q_c})\right]\left[i\cdot\omega - (i\cdot\omega_2 - \frac{\omega_2}{2Q_2})\right] + \mu^2}, \tag{7}$$

where $Q_c = \omega\tau_c/2$ and $Q_2 = \omega_2\tau_{i2}/2$; Q_c and Q_2 denote the total *Q* factor of the low-*Q* and high-*Q* cavities, respectively. Several typical power transmission ($T = |t|^2$) results obtained from Eq. (7) are plotted in Fig. 3, from which experimental results can be predicted. Figures 3(a)-3(c) denote weak coupling cases, in which the *Q* factor difference of the two cavities is designed to be sufficiently large. When $\omega_2 = 0.7\omega_1$ and $\omega_2 = 1.3\omega_1$, the results are plotted in Figs. 3(a) and 3(c), indicating the typical Fano-like resonance line shape with opposite symmetry. If $\omega_2 = \omega_1$, it is a special case of Fano-like interference, that is, EIT-like phenomenon, as shown in Fig. 3(b). When the two cavities are strongly coupled, mode splitting will happen instead of Fano-like interference as shown in Fig. 3(d), in which $\omega_2 = \omega_1$ and the two cavities have the same *Q* factor value.

Besides the prediction of Fano-like resonances, Eq. (7) can also be used to analyze the device parameters' effect on the resonance performance. Here the authors utilize parameters derived from the fabricated devices to predict the resonance performance. A typical resonance is plotted as the orange curve in Fig. 3(e). According to the discussion above, the *Q* factor of the low-*Q* cavity (Q_c) can be easily designed. It is found using Eq. (7) that a higher Q_c results in a sharper resonance slope and a higher maximum extinction ratio. For example, the pink transmission curve in Fig. 3(e), which is predicted from a device with a higher Q_c relative to the orange curve, has a larger slope and a higher maximum extinction ratio. It is also found that a higher value of μ (within a small range) has a similar effect as a higher Q_c. However, it can lead to strong coupling and mode splitting if the value of μ or Q_c is so high that the weak coupling condition is broken. These numerical results and discussion can serve as excellent design guidelines for devices with Fano-like resonances, which is missing in other literatures.

Optics EXPRESS

Generally speaking, a higher *Q* factor always makes a resonator's resonance slope sharper. However, in practice the *Q* factor of a resonator is limited because of fabrication tolerance, device roughness, material absorption and more. Thus, it is prudent to investigate how to enhance a resonance slope with a limited *Q* factor using for example, Fano-like resonances.

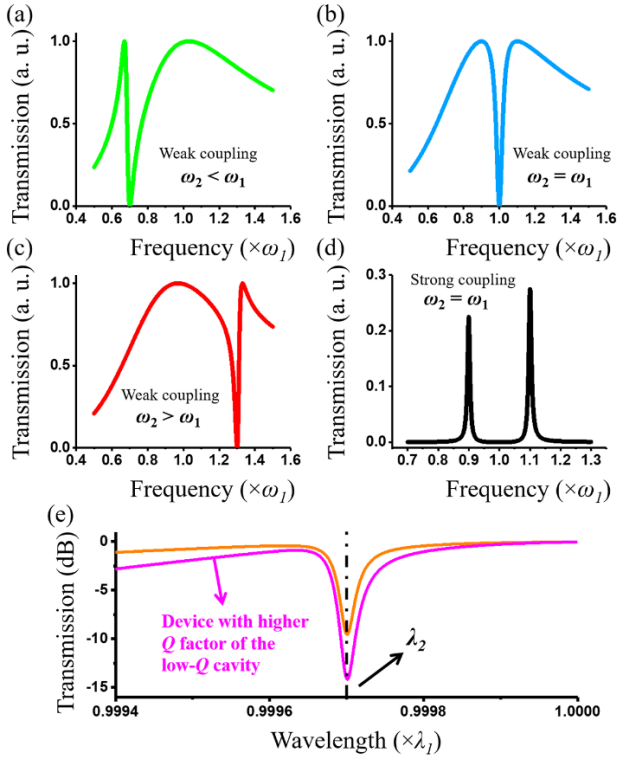

Fig. 3. Plotted power transmission results obtained from Eq. (7) for weak coupling cases with (a) $\omega_2 = 0.7\omega_1$, (b) $\omega_2 = \omega_1$ and (c) $\omega_2 = 1.3\omega_1$, and for (d) strong coupling case with $\omega_2 = \omega_1$. The transmission spectra are normalized to incident power. (e) Transmission results predicted using Eq. (7) with parameters derived from the fabricated devices. The pink curve denotes a transmission spectrum predicted with a higher Q_c relative to the orange curve. $\lambda_{1,2}$ denote the resonance wavelength of the two cavities.

3. Experimental results and discussion

The devices studied in this paper are illustrated in Fig. 4, which are fabricated on the 340 nm SOI platform. Figure 4(a) shows the prototype device (device A). The device (device B) in Fig. 4(b) is the bare high-*Q* cavity to be integrated in the prototype device, the schematic of which is given in Fig. 2(b). The PTE reflection coefficient is measured using device C in Fig. 4(c), the schematic of which is given in Fig. 2(c). These devices are mainly based on strip single mode waveguide having a width of 420 nm. The Sagnac loops are designed to have large diameters to reduce intrinsic loss; the MMIs are designed to work at 1550 nm. Some key dimensions of the loops and the MMIs are annotated in Fig. 4(a). The light input and output are realized through free-space coupling between optical fibers and on-chip grating couplers.

Optics EXPRESS

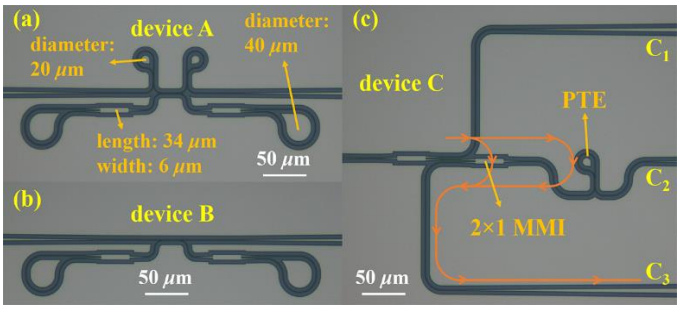

Fig. 4. Optical microscope images of the devices tested in this study. (a) The prototype device. (b) The high-*Q* cavity device to be integrated in the prototype device. (c) The device used to measure the reflection ratio of the PTE.

In experiments, the transmission spectrum of device B is plotted in Fig. 5(a). The measured *Q* factors of the resonances are approximately 13000. As to device C, the spectra measured at channel C_2 and C_3 are given in Fig. 5(b) and the reflection coefficient can be calculated as $2C_3/(C_2 + 2C_3)$). However, as can be seen, there are ripples on the spectrum of C_3, which is caused by the interference between the reflection from the 2 × 1 MMI and the reflection from the PTE. The interference forms unbalanced Mach-Zehnder-Interferometer-like (MZI-like) resonances and the corresponding optical path is annotated in Fig. 4(c). (It is verified using 3D finite-difference time-domain (FDTD) simulation that when light is launched into the 2 × 1 MMI from the upper input ports, a considerable amount of light can be collected from the lower input port.) Thus, the spectrum of C_3 can be processed by analyzing the extinction ratio and free-spectral-range (FSR) of the ripples. We process the spectra of both C_2 and C_3 by low pass filtering, the results of which are shown as the dashed curves in Fig. 5(b). The PTE reflection coefficient is calculated to be 0.35 at 1552 nm. The extinction ratio and the FSR of the ripples can be theoretically calculated and the results match the measured spectrum of C_3.

Next, a spectrum of the prototype device is given in Fig. 5(c), in which Fano-like resonances with different symmetries and EIT-like resonance can be observed. To link the experimental results with the theoretical analysis, the resonances of the low-*Q* cavity are also marked. As can be seen, when $\lambda_2 < \lambda_1$ the symmetry of the Fano-like resonance (marked as green) resembles that in Fig. 2(a), whilst when $\lambda_2 > \lambda_1$ the symmetry of the Fano-like resonance (marked as red) resembles that in Fig. 2(c). If $\lambda_2 \approx \lambda_1$, an EIT-like resonance (marked as blue) is observed resembling the spectrum in Fig. 2(b). (λ_i denotes resonant wavelength.) Note that the high-*Q* cavity has a smaller FSR. A Fano-like resonance is selected and re-plotted in Fig. 5(d). Using this resonance, a maximum intensity extinction ratio of 22.3 dB can be achieved with a wavelength detuning of just 54 pm as marked on the curve. By fitting the sharp line shape of this Fano-like resonance, the maximum slope can be obtained as high as 0.77 dB/pm, depicted as the red dashed line in Fig. 5(d). The fitting range covers an extinction ratio of 16.45 dB over 23 pm. The performance of the device in this study can be enhanced by optimizing the MMI design.

Finally, the effect of the *Q* factor of the low-*Q* cavity (Q_c) on the resonance performance is examined. In experiments, two devices are tested, one with an estimated Q_c of 170 and the other one with an estimated Q_c of 450. Fifteen Fano-like resonances within the wavelength range from 1545 nm to 1560 nm are measured on the two devices. The maximum slope values and the maximum extinction ratio values are averaged and plotted as the bars in Figs. 5(e) and 5(f). Figure 5(e) presents the results of the averaged maximum slope of both devices, whilst Fig. 5(f) presents the results of the averaged maximum extinction ratio. The red bars present the results of the device with lower Q_c (170), whilst the blue bars present the results of the device with

Optics EXPRESS

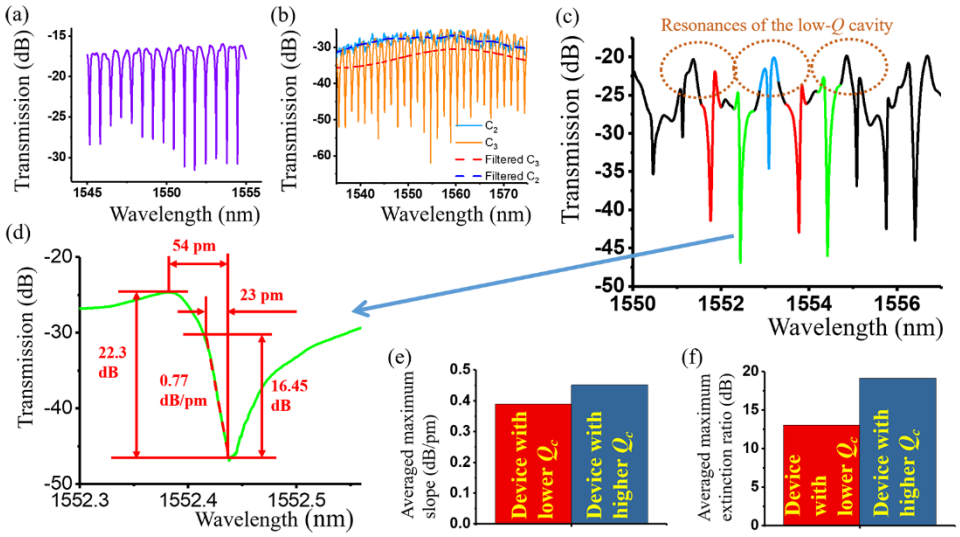

Fig. 5. Experimental results. The transmission spectra are normalized to the incident power. (a) Spectrum acquired from device B to characterize the *Q* factor of the high-*Q* cavity. (b) Spectra acquired from device C to measure the reflection ratio of the PTE. Dashed lines are obtained through filtering interference fringes. (c) Spectrum of the prototype device (device A) to present the Fano-like resonance investigated in this study. A typical resonance on the spectrum in (c) is selected and re-plotted in (d), in which the sharp slope is fitted as the red dashed line. (e and f) Averaged maximum slope results and averaged maximum extinction ratio results measured from a device with lower Q_c value (presented by the red bars) and a device with higher Q_c (presented by the blue bars).

higher Q_c (450). As can be seen, higher Q_c results in higher resonance slope and higher extinction ratio, which verifies the theoretical prediction in Section 2.

4. Conclusions

In summary, this study experimentally demonstrates an ultra-sharp Fano-like resonance mechanism, which is supported by a theoretical analysis. The authors establish a model of weakly dual-coupled FP cavities, one with high-*Q* factor and the other one with low-*Q* factor. By analytically and numerically investigating this model, the authors develop a guideline to design devices with Fano-like resonance. Based on these theoretical studies, experiments are designed and conducted, the results of which successfully match the theoretical results. In the experiments, the slope of the sharp resonance line shape is measured as high as 0.77 dB/pm, which is the highest among the literature based on on-chip integrated Si photonic devices, to the best of the authors' knowledge. Crucially, the prototype device is patterned using DUV lithography only and does not require ultra-high resolution lithography techniques such as electron-beam lithography, which demonstrates the fabrication feasibility for such Si photonic devices with Fano-like resonances using conventional CMOS compatible foundry services.

Funding

Engineering and Physical Sciences Research Council (EPSRC) CORNERSTONE project (EP/L021129/1); National Research Foundation of Singapore (NRF-CRP12-2013-04).

Acknowledgments

The authors would like acknowledge the CORNERSTONE [26] platform, through which the prototype device is fabricated. C. G. Littlejohns acknowledges support from National Research Foundation of Singapore. D. J. Thomson acknowledges funding from the Royal Society for his

Optics EXPRESS

University Research Fellowship. All data supporting this study are available upon request from the University of Southampton repository at http://doi.org/10.5258/SOTON/D0700.

References

1. U. Fano, "Effects of configuration interaction on intensities and phase shifts," Phys. Rev. **124**(6), 1866–1878 (1961).
2. B. Peng, Ş. K. Özdemir, W. Chen, F. Nori, and L. Yang, "What is and what is not electromagnetically induced transparency in whispering-gallery microcavities," Nat. Commun. **5**(1), 5082 (2014).
3. M. F. Limonov, M. V. Rybin, A. N. Poddubny, and Y. S. Kivshar, "Fano resonances in photonics," Nat. Photonics **11**(9), 543–554 (2017).
4. Y. Shuai, D. Zhao, A. Singh Chadha, J.-H. Seo, H. Yang, S. Fan, Z. Ma, and W. Zhou, "Coupled double-layer Fano resonance photonic crystal filters with lattice-displacement," Appl. Phys. Lett. **103**(24), 241106 (2013).
5. W. Zhang and J. Yao, "Thermally tunable ultracompact Fano resonator on a silicon photonic chip," Opt. Lett. **43**(21), 5415–5418 (2018).
6. K. Nozaki, A. Shinya, S. Matsuo, T. Sato, E. Kuramochi, and M. Notomi, "Ultralow-energy and high-contrast all-optical switch involving Fano resonance based on coupled photonic crystal nanocavities," Opt. Express **21**(10), 11877–11888 (2013).
7. X. Yang, C. Husko, C. W. Wong, M. B. Yu, and D. L. Kwong, "Observation of femtojoule optical bistability involving Fano resonances in high-Q/V-m silicon photonic crystal nanocavities," Appl. Phys. Lett. **91**(5), 051113 (2007).
8. Y. Yu, M. Heuck, H. Hu, W. Q. Xue, C. Peucheret, Y. H. Chen, L. K. Oxenlowe, K. Yvind, and J. Mork, "Fano resonance control in a photonic crystal structure and its application to ultrafast switching," Appl. Phys. Lett. **105**(6), 061117 (2014).
9. D. A. Bekele, Y. Yu, H. Hu, P. Guan, M. Galili, L. Ottaviano, L. K. Oxenløwe, K. Yvind, and J. Mork, "Signal reshaping and noise suppression using photonic crystal Fano structures," Opt. Express **26**(15), 19596–19605 (2018).
10. Y. Yu, Y. Chen, H. Hu, W. Xue, K. Yvind, and J. Mork, "Nonreciprocal transmission in a nonlinear photonic-crystal Fano structure with broken symmetry," Laser Photonics Rev. **9**(2), 241–247 (2015).
11. J. H. Zhang, X. Leroux, E. Duran-Valdeiglesias, C. Alonso-Ramos, D. Marris-Morini, L. Vivien, S. L. He, and E. Cassan, "Generating Fano Resonances in a Single-Waveguide Silicon Nanobeam Cavity for Efficient Electro-Optical Modulation," ACS Photonics **5**(11), 4229–4237 (2018).
12. A. D. Osterkryger, J. R. de Lasson, M. Heuck, Y. Yu, J. Mørk, and N. Gregersen, "Spectral symmetry of Fano resonances in a waveguide coupled to a microcavity," Opt. Lett. **41**(9), 2065–2068 (2016).
13. L. Zhou and A. W. Poon, "Fano resonance-based electrically reconfigurable add-drop filters in silicon microring resonator-coupled Mach-Zehnder interferometers," Opt. Lett. **32**(7), 781–783 (2007).
14. F. Wang, X. Wang, H. Zhou, Q. Zhou, Y. Hao, X. Jiang, M. Wang, and J. Yang, "Fano-resonance-based Mach-Zehnder optical switch employing dual-bus coupled ring resonator as two-beam interferometer," Opt. Express **17**(9), 7708–7716 (2009).
15. M. Galli, S. L. Portalupi, M. Belotti, L. C. Andreani, L. O'Faolain, and T. F. Krauss, "Light scattering and Fano resonances in high-Q photonic crystal nanocavities," Appl. Phys. Lett. **94**(7), 071101 (2009).
16. W. Bogaerts, R. Baets, P. Dumon, V. Wiaux, S. Beckx, D. Taillaert, B. Luyssaert, J. Van Campenhout, P. Bienstman, and D. Van Thourhout, "Nanophotonic waveguides in silicon-on-insulator fabricated with CMOS technology," J. Lightwave Technol. **23**(1), 401–412 (2005).
17. W. Bogaerts, D. Taillaert, B. Luyssaert, P. Dumon, J. V. Campenhout, P. Bienstman, D. V. Thourhout, R. Baets, V. Wiaux, and S. Beckx, "Basic structures for photonic integrated circuits in Silicon-on-insulator," Opt. Express **12**(8), 1583–1591 (2004).
18. W. Bogaerts, V. Wiaux, D. Taillaert, S. Beckx, B. Luyssaert, P. Bienstman, and R. Baets, "Fabrication of photonic crystals in silicon-on-insulator using 248-nm deep UV lithography," IEEE J. Sel. Top. Quantum Electron. **8**(4), 928–934 (2002).
19. A. Li and W. Bogaerts, "Tunable electromagnetically induced transparency in integrated silicon photonics circuit," Opt. Express **25**(25), 31688–31695 (2017).
20. Q. Li, T. Wang, Y. Su, M. Yan, and M. Qiu, "Coupled mode theory analysis of mode-splitting in coupled cavity system," Opt. Express **18**(8), 8367–8382 (2010).
21. H. Du, X. Zhang, G. Chen, J. Deng, F. S. Chau, and G. Zhou, "Precise control of coupling strength in photonic molecules over a wide range using nanoelectromechanical systems," Sci. Rep. **6**(1), 24766 (2016).
22. Y. Sato, Y. Tanaka, J. Upham, Y. Takahashi, T. Asano, and S. Noda, "Strong coupling between distant photonic nanocavities and its dynamic control," Nat. Photonics **6**(1), 56–61 (2012).
23. M. J. Hartmann, F. G. S. L. Brandao, and M. B. Plenio, "Strongly interacting polaritons in coupled arrays of cavities," Nat. Phys. **2**(12), 849–855 (2006).
24. X. Sun, L. Zhou, J. Xie, Z. Zou, L. Lu, H. Zhu, X. Li, and J. Chen, "Tunable silicon Fabry-Perot comb filters formed by Sagnac loop mirrors," Opt. Lett. **38**(4), 567–569 (2013).
25. Y. Xu, Y. Li, R. K. Lee, and A. Yariv, "Scattering-theory analysis of waveguide-resonator coupling," Phys. Rev. E Stat. Phys. Plasmas Fluids Relat. Interdiscip. Topics **62**(5 5 Pt B), 7389–7404 (2000).
26. *http://www.cornerstone.sotonfab.co.uk/*, accessed on 02/11/18.